An Autonomously Recording Inverted Echo Sounder: ARIES II

S. A. THORPE, M. J. ULLOA, AND D. BALDWIN

Department of Oceanography, Southampton Oceanography Centre, University of Southampton, Southampton, United Kingdom

A. J. HALL

George Deacon Division for Ocean Processes, Southampton Oceanography Centre, Southampton, United Kingdom

(Manuscript received 10 June 1997, in final form 24 November 1997)

ABSTRACT

A self-contained instrument, the Autonomously Recording Inverted Echo Sounder (ARIES II), carrying two 250-kHz beam side-scan sonars and with the capacity to record sonar data sampled at 3.2 kHz for 168 h with the sonars operating with a pulse repetition rate of 2 Hz, has been constructed and tested in a mooring deployment that lasted for 25 days near the edge of the continental shelf west of Scotland. The mean water depth was 146 m. ARIES II was positioned at a mean transducer depth of 34.6 m with sonars directed upward at 20° to the horizontal to obtain acoustic returns from targets at or near the sea surface. The instrument was preprogrammed to record continuously over periods of 2, 4, and 13 h, the last to cover the M2 tidal cycle dominant in the area.

Sonographs are presented to illustrate observations of surface waves and wave groups, internal solitons, rain showers, and Langmuir circulation. An analysis is made of the effects of surface waves, currents, and internal waves on the instrument. The potential use of the instrument is demonstrated in providing estimates of the propagation direction and speed of internal waves, as well as in estimating the drift, orientation, and mean separation of Langmuir bands. The separation is found to increase with wind speed.

1. Introduction

The use of upward-pointing sonar as a means to investigate the upper ocean has developed rapidly in the last 15 years. It has proved to be a useful means of collecting information about surface waves, particularly their breaking and the bubble clouds they create, surface currents, internal waves, and Langmuir circulation (see, e.g., Thorpe and Hall 1983; Zedel and Farmer 1991). Many of the observations, however, are restricted by the lack of a system with independent power and large data capacity that can operate, unattended, for long periods and so collect continuous data in extreme conditions or from hazardous locations, such as those in which vessels can gain access only in ice-free or calm conditions.

The Autonomously Recording Inverted Echo Sounder (ARIES II) (Fig. 1) is an autonomous, upward-pointing, two-beam, 250-kHz side-scan sonar that is capable of internally recording sonar data sampled at 3.2 kHz for 168 h with a pulse repetition rate on both beams of 2 Hz. Also recorded at 2 Hz are temperature, pressure, and three angles—heading, pitch, and sideway tilt. It is a successor of a vertically pointing, narrow sonar beam instrument, ARIES, used to monitor bubble clouds in the Irish Sea and near the edge of the U.K. continental shelf (Thorpe 1986).

The new instrument is 1.9 m high, 0.36 m wide, and 1.8 m long. It weighs 230 kg in air and has a positive buoyancy of 84 kg in water. It is moored on a swivel from the lowest point about which it can rotate and is streamlined to orientate into the local flow and so minimize drag. It is capable of operation to depths of 200 m. Two sonar transducers are mounted on the upper surface of the casing forward of a surface-activated flashing light and an ARGOS beacon to aid location on recovery. In the trials described below and that illustrate the use of the instrument, the two side-scan sonar beams are set at 90° to each other, and each is directed at 20° above the horizontal toward the water surface. The beams are 33° wide in the vertical and 1.6° wide in the horizontal (beam angles measured to the −3-dB points). One points forward, into the relative current direction, and the other to starboard. The side-scan transducers have elements made from composite lead zirconate titanate (PZT), their source level is 171 dB re μPa/V at 1 m, and the receiver sensitivity is −182 dB re V/μPa. The electrical power into the transducers is 210 W (rms), and the pulse length is 275 μs. The effective target range resolution is about 0.25–185 m. The sonars are uncalibrated, but the sonographs described below provide

Corresponding author address: Dr. S. A. Thorpe, Department of Oceanography, University of Southampton, Waterfront Campus, European Way, Southampton SO14 3ZH United Kingdom.

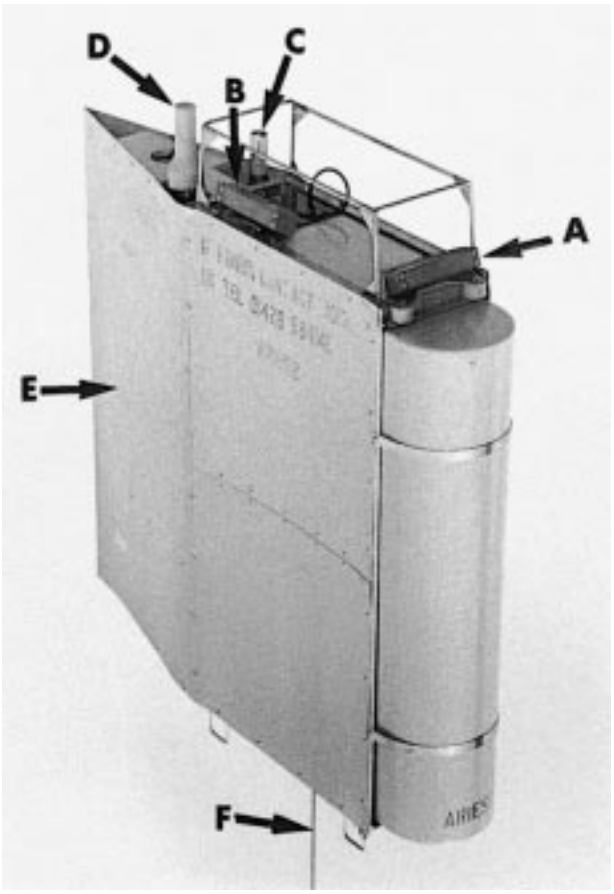

FIG. 1. ARIES II. The instrument case is 1.9 m high. The photograph shows the following: A, B, the forward and starboard sonar tranducers, respectively; C, the flashing light; D, the ARGOS beacon; E, the tapered fin that helps align the body of the instrument into the flow and reduce drag; and F, the wire that secures the instrument to the seabed.

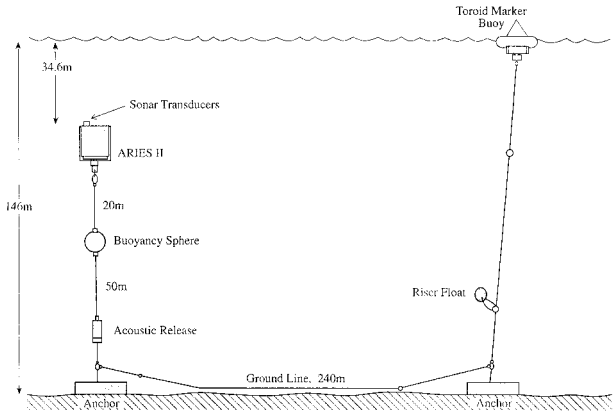

FIG. 2. The mooring. ARIES II could be recovered either by separating the acoustic release or by recovering the toriod marker buoy and ground line.

graphic illustration of the variety of features detectable at the sea surface. The temperature and pressure sensors are located at 1.52 and 1.49 m, respectively, below the sonar transducers. Data at 6.1 kbyte s^{-1} are transferred using DMA to the host computer, an Ampro 25-MHz 386SX. Data storage is via an SCSI interface to a shock-mounted 4-Gbyte hard disk that can be downloaded onto DAT tapes or optical disks. The operating times and durations are preselectable. The system requires a power capacity of 8 kW h. This is provided by a 135-cell lithium ($Li/SOCl_2$) pack with an output of 54 V and a specified capacity of 243 A h.

2. Deployment

ARIES II was deployed on a ''U mooring'' (Fig. 2) on 11 August 1995 at a mean acoustic transducer depth of 34.6 m in a water depth of 146 m at 56° 27.45′N, 08°58.09′W west of Scotland. The 160-m depth contour running roughly north–south and marking the edge of the continental shelf lies 3.5 km farther to the west. The site is exposed to the North Atlantic to the west and is an area of internal wave soliton activity [(Fedorov and Ginsberg 1986; Small et al. 1998); the latter describes observations of the horizontal density structure in the area and its modification by internal waves.] The slope current (Huthnance 1986) is centered approximately above the 500-m isobath, some 10 km west of the mooring. The measurement periods over 20 days, for which the system continued to operate, were set to 2, 4, and 13 h, the last to sample throughout the locally dominant M2 tide. Some previous use of the battery pack limited the recording time to 144 h. ARIES II was recovered on 5 September 1995.

Temperature and salinity structure at the site was obtained from conductivity–temperature–depth (CTD) stations. A mixed layer at 16°C extended typically to about 20 m, beyond which there was a thermocline about 15 m thick, with maximum temperature gradients of 0.6°C m^{-1} and a maximum buoyancy frequency of 0.02 s^{-1}. The temperature in the lower layer was fairly uniform at about 10°C. ARIES II was at a depth below the largest temperature gradients. Meteorological data in the earlier part of the deployment are available from ship measurements, but for the period from 17 August until the end of the deployment period they are sampled by a nearby meteorological buoy. The wind speeds during sampling periods ranged from near calm to 13 m s^{-1}.

A second mooring, carrying current meters at 30 and 55 m, sampling at 10- and 5-min intervals, respectively, was deployed about 0.6 km from the ARIES II mooring. The mean currents at 30 and 55 m during the ARIES II recording period (12–30 August) are 2.2 cm s^{-1} to 164° and 1.3 cm s^{-1} to 141°, respectively. Fluctuations are dominated by the tides, with typical current speeds of 0.1–0.2 m s^{-1} and amplitudes of 1 m, and by packets of internal waves traveling toward the east from the shelf break that induce currents of typically 0.05 m s^{-1}. The waves appear as a series of temperature maxima, typically 2 K above ambient at 55 m, implying a downward

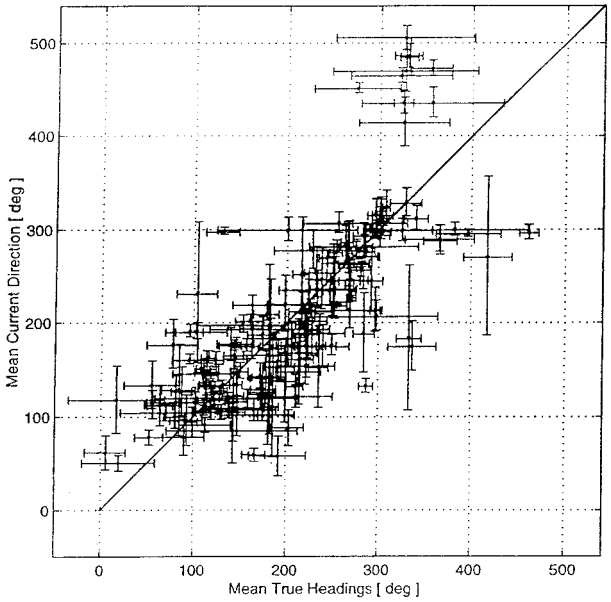

FIG. 3. The mean direction of current indicated by the alignment of ARIES II at 34.6 m vs the depth-weighted mean current directions from current meters at 30 and 55 m on a nearby mooring. Means are taken over half-hour periods. The groups of ''high'' points with mean current direction of 400°–500° (the scale is rolled over beyond 360°) and the ''low'' points with mean true headings at 400°–500° and near 330° are all associated with times at which internal waves were passing the moorings.

movement of near-surface water in a series of narrow wave troughs in the thermocline, 5–20 m deep (see, e.g., Apel et al. 1985; Sandstrom and Elliott 1984).

The ability of ARIES to orientate into the mean current is demonstrated in Fig. 3. This shows half-hour mean directions of ARIES II plotted against the depth-weighted mean directions measured by the current meters at 30 and 55 m. The rms scatter of points is about 45°, much of which is accounted for by the rms scatter of the measurements within the half-hour periods and by the horizontal and vertical spatial variability as the internal waves pass the two moorings (see section 5b).

3. Sonographs

Sonographs, plots of time versus range of the sound echoes received from targets in the sonar beams, are produced from the two sonars. The configuration of a single beam is shown in Fig. 4. The range r, depth of the instrument d, and range x measured along the surface from a point immediately above ARIES II are related by $r^2 = d^2 + x^2$. A target moving at constant speed u along the surface and in a fixed beam has position $x = ut$ if $x = 0$ at $t = 0$. Its range r is given by $r^2 - (ut)^2 = d^2$, which is a hyperbola in the $(r - t)$ frame of reference of the sonographs. The asymptotes are $r = \pm ut$, and the hyperbola is tangential to the surface at the apex, $r = d$. Range is determined from the time

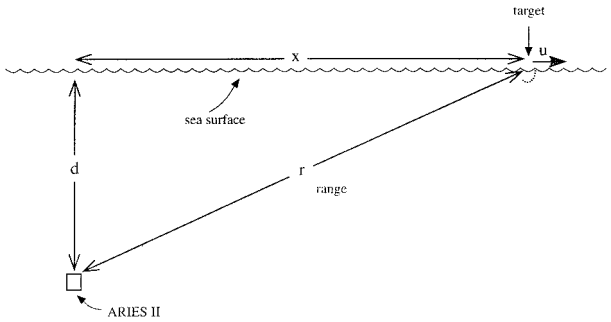

FIG. 4. The relation between the depth d of the ARIES II sonar transducers, the range r of a target, and the horizontal range of the target x. The depth d can be measured directly from the sonar's sideband echo from the sea surface.

delay, assuming a constant speed of sound, nominally taken as 1500 m s^{-1}.

a. Long period sonographs: Tides and internal waves

Figure 5 shows data obtained from ARIES II over a 13-h period. Figures 5a and 5b are sonographs obtained from the two beams. Figures 5c–e show water temperature, pressure, and heading of the forward beam, respectively. The wind speed was 8.5 m s^{-1} from 263°. The sea surface, at a range corresponding to that derived from the pressure record, appears as a strong target at about 35-m range. The range and pressure follow sinusoidal variations that are in phase and have equal amplitude. These correspond to the surface tide in the area. Acoustic targets visible in the sonographs at ranges less than that of the sea surface are located beneath the surface. These appear to be of two kinds. Small, discrete targets of short time duration (typically a few seconds) are believed to be fish. (The area is one of active fishing.) More extensive targets that persist for a minute or more are detected when the troughs of large soliton-type internal waves, apparent in the temperature record (Fig. 5c), pass the instrument (e.g., at times 4–6.5 h; see also Fig. 13). The scatterers associated with the internal waves probably mark the presence of zooplankton near the surface that is carried closer to the instrument in the internal wave troughs, thus contributing to high local scatter and attenuating the signal from greater ranges. Several of the waves have double temperature maxima and, correspondingly, two bands of scatterers. The cause is not obvious, but it could be that the mooring is in a region of crossing internal wave packets. These are clearly visible in *ERS-2* synthetic aperture radar (SAR) images of the area (Small et al. 1998). At other times (e.g., see Fig. 13 and section 5b), single temperature peaks are observed. The presence of the internal waves is also evident in the variations of amplitude 0.1 m in instrument depth (see Fig. 5d). Their acoustic refraction is discussed in section 4a.

Figure 6 shows the currents at 30 and 55 m and the temperature fluctuations at 55 m measured at the nearby

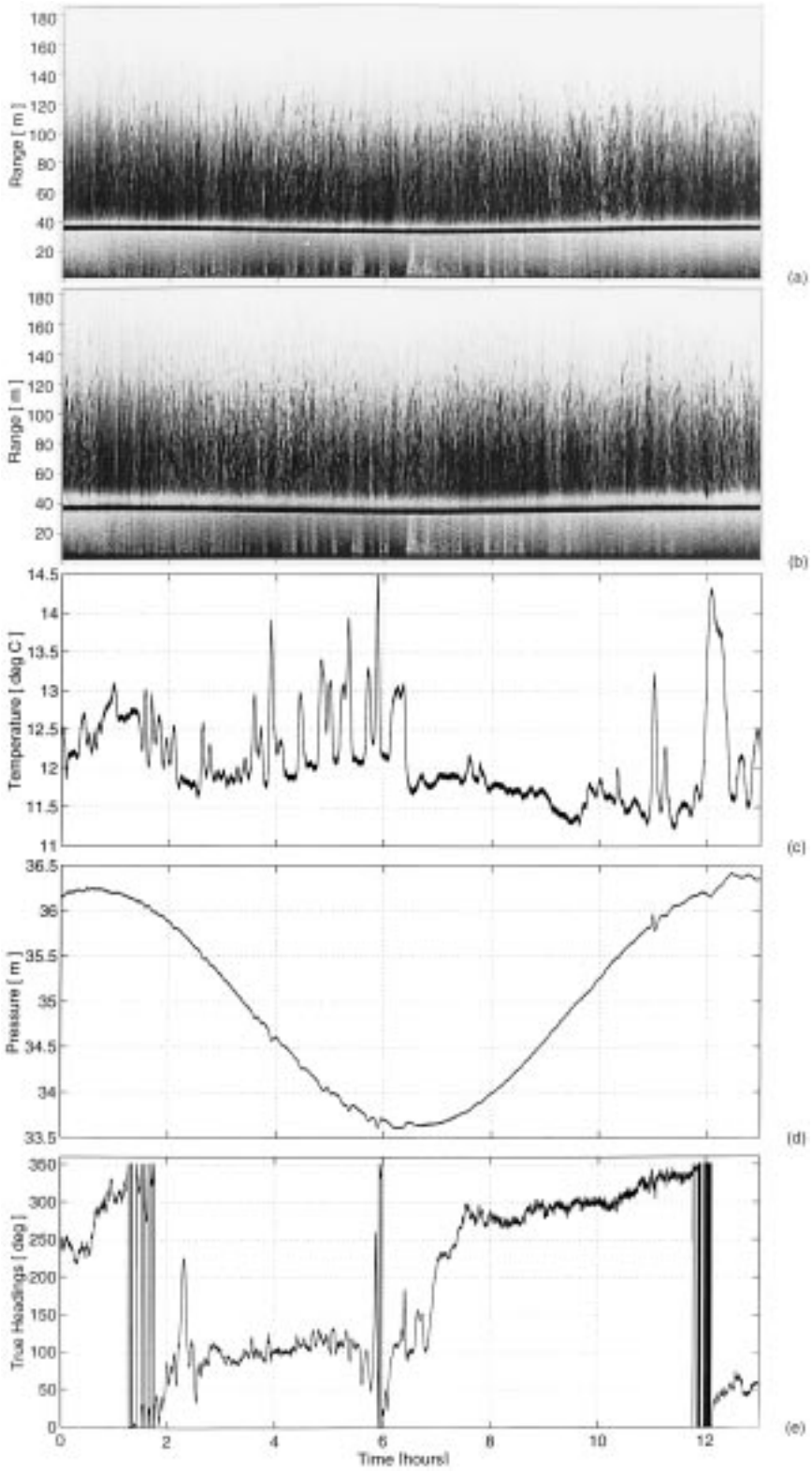

FIG. 5. (a) The forward beam sonograph and (b) the starboard beam sonograph, each range vs time with stronger targets marked with darker shades of gray, obtained from ARIES II over a period of 13 h together with (c) the ARIES II–recorded water temperature, (d) the pressure (corrected to the level of the sonar tranducers and averaged over 1 min), and (e) the heading of the forward beam. The mean wind speed is 8.5 m s^{-1} from 263°. The record begins at 0814 GMT 15 August 1995.

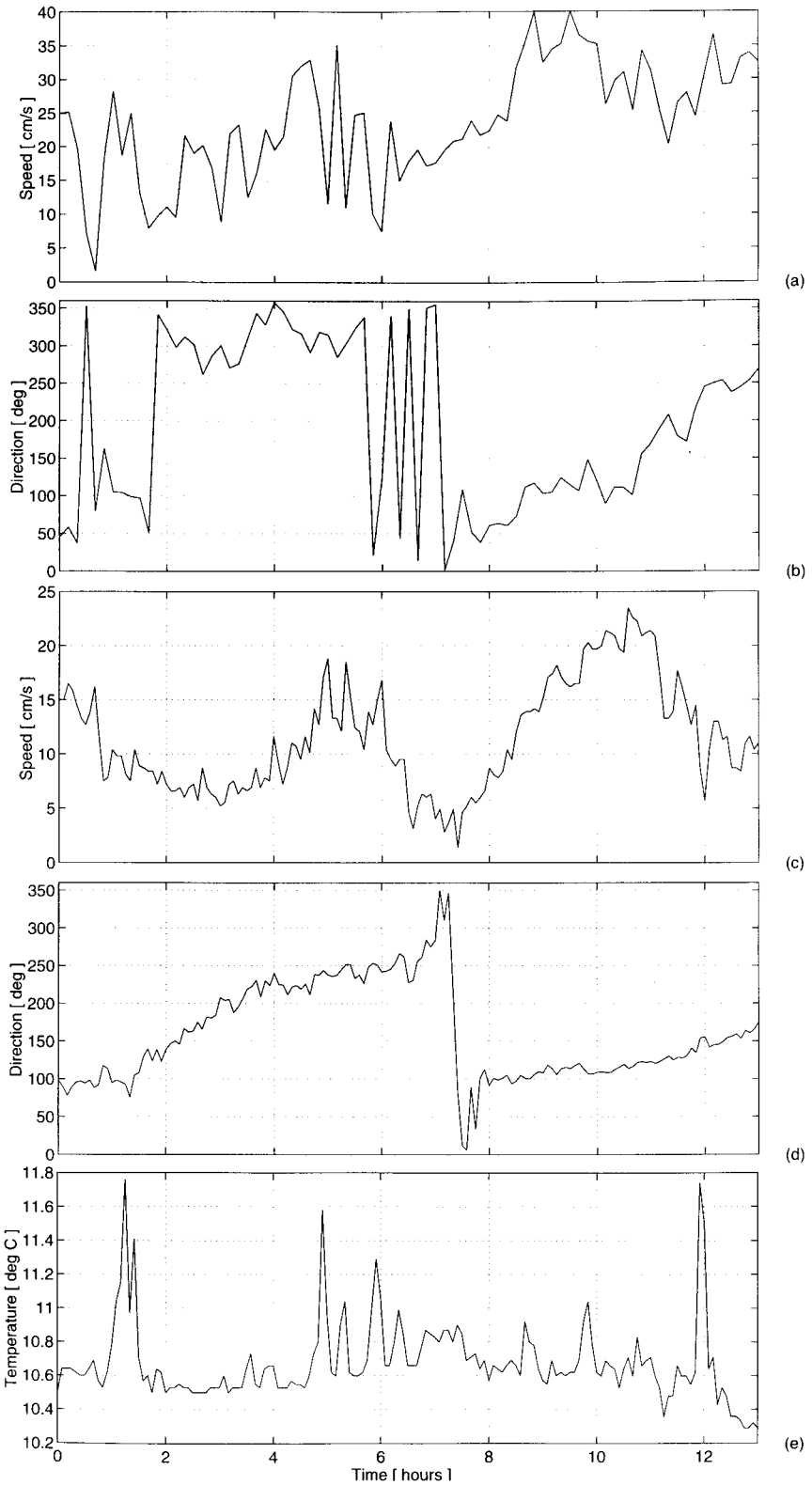

FIG. 6. Currents and direction for the same period as in Fig. 6 measured at [(a) and (b)] 30 m and [(c) and (d)] 50 m at the nearby mooring. (e) The temperature at 55-m depth. A vertical gradient in current speed and direction is evident. The direction in Fig. 5e is that in which the sonar beam is pointing and is therefore *contrary* to the current direction (see Fig. 3).

mooring. The internal wave train is evident in the record, but the time resolution, 10 min at 30 m and 5 min at 55 m, is insufficient to reveal the presence or absence of the double temperature peaks. The wave train is accompanied by flows at both levels with westerly components. It produces current fluctuations of 5–20 cm s^{-1} and precedes an increase in flow speed and rapid change in direction at 7.5 h to an eastward flow at both levels. (The current directions are roughly opposite to the heading of the forward beam shown in Fig. 5e.) The current changes associated with the internal waves indicate eastward pulses at 30 m, decreasing the westward flow component, and smaller westward motions at the lower, 55-m instrument, indicating eastward-propagating soliton waves. The current changes and consequent variations in drag appear to be responsible for the ''knockdown'' and small depth increase of ARIES II as the waves pass. Internal waves may themselves contribute to a vertical rise in sea surface level over their wave troughs (Peters and Stoker 1960), but even in the extreme case of a two-layer fluid with the observed CTD density differences and internal waves of 20-m height, the surface elevation would increase over the wave troughs by only about 0.02 m.

Beyond the range of the surface, scattering is from targets in the water and from the sea surface. It is known that the strongest and most common near-surface targets in windy weather are the bubble clouds formed by breaking wind waves. Their scattering cross section falls off rapidly with depth. The typical *e*-folding scale is about 0.5 m, increasing to 1 m in winds of 15 m s^{-1} (Thorpe 1984a). Individual bubble clouds are not resolved in Fig. 5. The variations in scattering intensity with range, at ranges beyond that of the surface, arise from the beam pattern that, directed up at 20°, leads to a reduction in scattering immediately after the surface return and then to an increase to maximum at a range of about 65 m before the gradual reduction caused by sound attenuation at greater ranges. Variations of scattering intensity with time result from such factors as changes in sea surface roughness and bubble production, changes in beam orientation as the instrument direction changes in response to currents, and changes resulting from the attenuation of sound reaching the surface by the presence of subsurface scatterers.

b. High-resolution sonographs: Langmuir circulation and surface waves

Figure 7 shows sonographs and accompanying data for a period of 2 min. At this time resolution, fluctuations caused by surface waves are visible in the range of the surface target near 40 m. Both low-frequency (e.g., at A, 80 s into the record; period $\approx$ 11.3 s) and higher-frequency (e.g., B at 45 s; period about 4–5 s) waves are evident. The low-frequency waves are also apparent in the pressure record as well as in the heading and inclinometer records, although with some phase change. At greater ranges, two patterns are evident. There are slightly tilted bands with separations of a few meters, seen most clearly in the starboard sonograph (e.g., at C and D in Fig. 7b). In both sonographs the bands approach the sonar (range decreases with time). The range of these bands has a periodic variation at a frequency of the low-frequency waves. These bands are lines of bubbles resulting from the advection of bubbles produced by breaking waves into the zones of convergence created by Langmuir circulation (Thorpe 1984b; Zedel and Farmer 1991; Farmer and Li 1994); the bands of bubbles lie along the convergence lines. The second pattern that is apparent is that of inclined bands, which are best seen in the forward sonograph (e.g., at E and F in Fig. 7a), where they approach the sonar. These bands are composed of many short, less-tilted streaks (best seen at E), and there is evidence that the streaks have a higher frequency than the bands (e.g., at 45-m range at 45–65 s, or at 170-m range at 30–35 s), the near-vertical streaks reoccurring with a period of a few seconds. The bands and streaks are the result of sound scatter from the tilted surfaces of surface waves. The main bands of scatterers, marking the long-period swell waves that approach the forward sonar at approximately constant phase speed, have the hyperbolic paths predicted in section 3a. The hyperbolic scattering bands meet the surface echoes in positions that, in time, precede a wave trough. The scattering, therefore, comes from the backward face of the swell, the region near the node that follows the crest and in which the mean surface of the long waves is most nearly normal to the direction of the sonar beam. The tilt of the mean surface associated with the larger waves is, however, insufficient to bring them normal to the sonar beam at the larger ranges, and the sonar signals are strengthened by returns from the shorter waves riding on the swell with lower phase speeds. This accounts for the streaks that make up the bands; acoustic scattering results from specular reflection from the smaller waves riding on or over the larger swell waves.

The fluctuations in pressure and heading are mainly dominated by the swell, but small-amplitude fluctuations with a period of about 1–2 s are seen that may result from eddy shedding from the body of the instrument.

Figure 8 shows the general effect of increasing wind speed on the sonograph images. The images are plotted on a common intensity scale and are unquantified since the sonar is uncalibrated. The sonographs are 10 min long, and the beam and wind directions are given in the figure caption. The amplitude of the surface waves, seen on the surface at ranges of about 36 m in the sonographs and approaching or retreating from the sonar at greater ranges, increases with wind speed, and the presence of wave groups becomes more evident as wind increases. Beyond the range of the surface, the linear scattering bands caused by Langmuir circulation are visible and become stronger and more widely spaced as wind in-

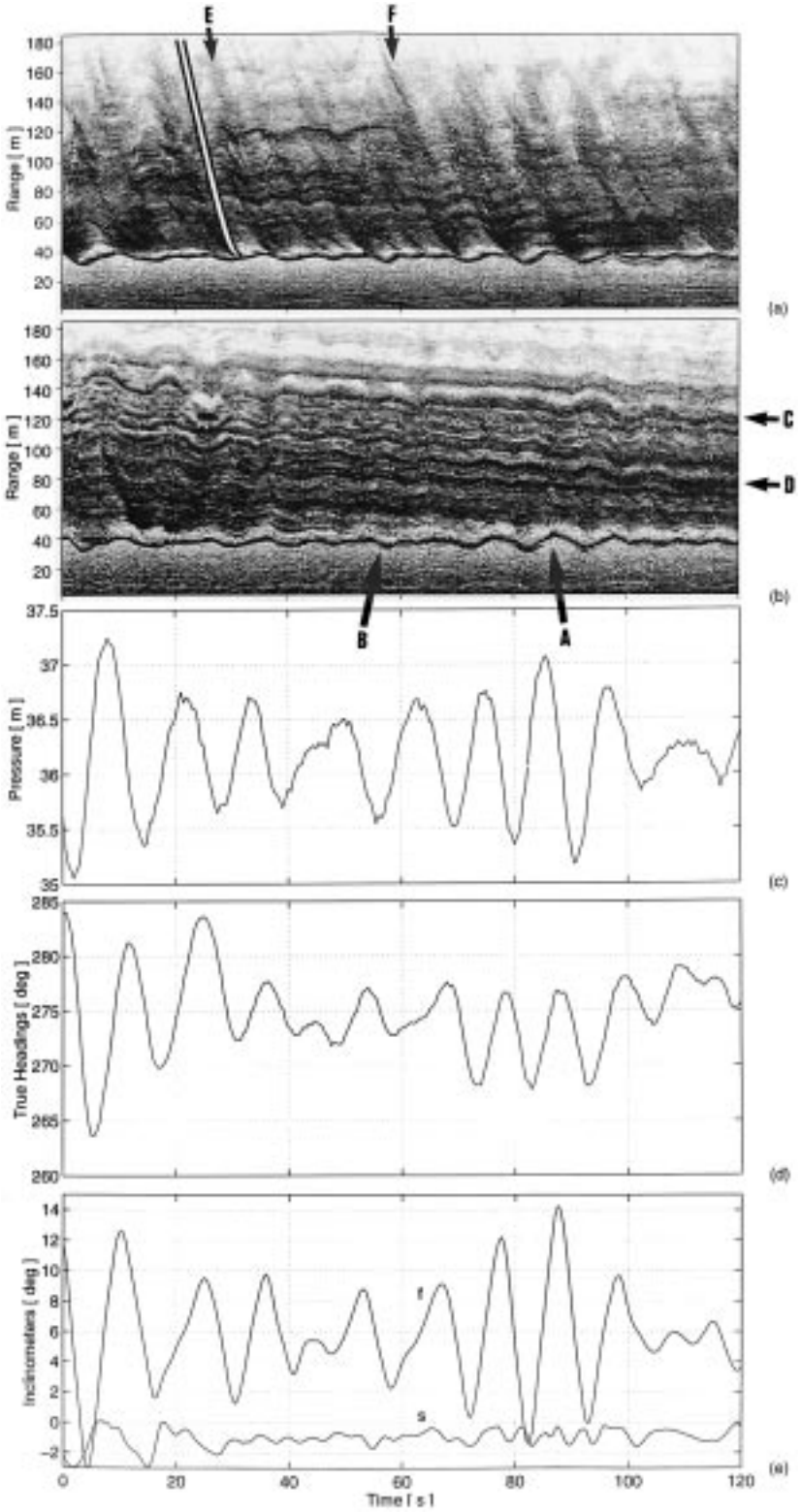

FIG. 7. A 2-min period showing surface waves and Langmuir bands: (a) forward sonograph, (b) starboard sonograph, (c) pressure, (d) direction of forward beam, and (e) the fore–aft (marked f; positive is ''nose up'') and lateral (marked s; negative is a tilt down to starboard) inclinometers. The mean wind speed is 12.7 m s^{-1} in direction 40° ± 20°. The hyperbola superimposed on the forward sonograph image is explained in section 4d(1). Letters A–E are explained in text. The record begins at 0614 GMT 25 August 1995.

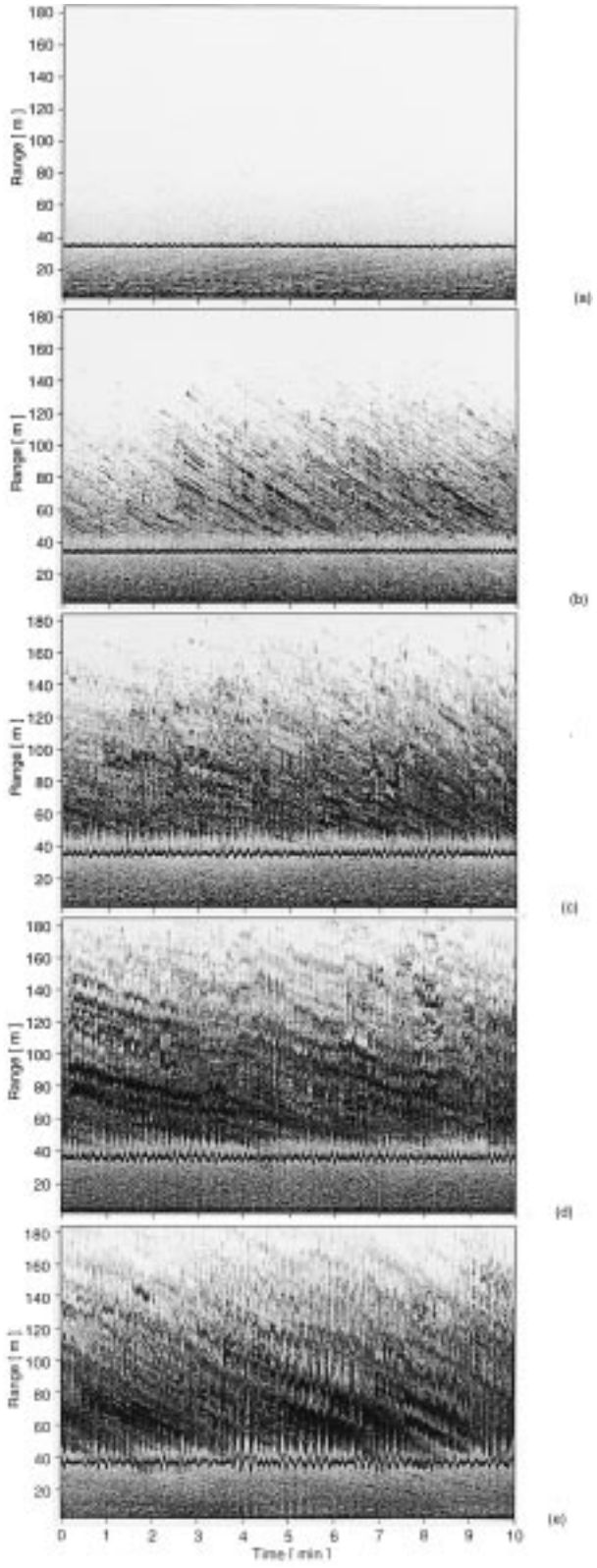

FIG. 8. Sonographs taken at different wind speeds W_{10} in order of increasing wind speed. Values of W_{10} (m s^{-1}), wind direction θ_{wi} (°), and beam orientation θ_{be} (°), in respective order, are as follows: (a) 1.9 ± 0.1, 249 ± 19, 349 ± 8; (b) 4.7 ± 0.3, 351 ± 3, 258 ± 5; (c) 7.7 ± 0.2, 47 ± 3, 278 ± 31; (d) 11.2 ± 0.2, 351 ± 12, 96 ± 6; and (e) 13.1 ± 0.1, 51 ± 9, 308 ± 10. The uncertainty indicated is the rms variation about the mean value. The sonographs are all on the same scale of scattering intensity. This results in some loss of detail at the lower wind speeds and at higher range where, with enhanced contrast, linear bands are still visible. The records begin at (a) 1520 GMT 19 August, (b) 1520 GMT 30 August, (c) 0700 GMT 23 August, (d) 1930 GMT 24 August, and (e) 0640 GMT 25 August (all in 1995).

creases (see Table 1). Their spacing and orientation are discussed in section 5c.

The Langmuir bands seen in Fig. 7 and Figs. 8d,e appear to fluctuate in range over periods comparable to those of the surface waves. Several effects influence the appearance of features seen in the sonographs, and these are discussed in section 4.

4. Factors affecting the sonograph images

a. The effect of temperature variations on the sonar beam

The sonographs have been generated making the assumption of a constant speed of sound and taking no account of the increase of sound speed with temperature as sound propagates through the thermocline nor any account of variations caused by the redistribution of temperature—and hence sound speed—in the water column by internal waves. Refraction through the thermocline leads to a mean distortion of acoustic paths and downward reflection of rays propagating from the source at less than about 10° to the horizontal. Refraction may, however, be more severe when steep internal waves are passing through the sonar beams. The errors in estimating the range of reflecting targets at the surface is less than 1.1% to ranges of 250 m. The largest internal wave troughs observed are found to result in an apparent reduction in the range of the water surface by about 0.2 m, an estimate of the errors involved in neglecting the variation in temperature on the depth of the transducers. These effects are generally small in comparison with those described below.

b. The motion of bubble bands and beam rotation

Consider a band of bubbles, or set of bands, within the sonar beam that are moved laterally at speed V and that intersect the forward beam at angle ϕ (Fig. 9a). The rate of change in time of the position of the bands along the line of intersection of the forward and starboard beams with the surface are $V/\sin\phi$ and $V/\cos\phi$, respectively. Each can be measured from the slope of the bands seen in the sonographs (with due attention to determining the changes in position along the surface, x, in Fig. 4, rather than range). Their ratio gives $\tan\phi$, and V can also be found. It is not necessary to suppose that the bands are of length sufficient for them to appear

TABLE 1. The variations of Langmuir band orientation, θ_b (°), found from (1), the lateral advection speed, V (cm s^{-1}), of the bands estimated using (2), and mean band separation, S (m), with wind speed, W_{10} (m s^{-1}), and direction, θ_{wi} (°), and with surface waves. The sign ascribed to V is positive for bands migrating to the right of the alignment direction θ_b, and negative to the left. Wind data and their standard deviation are derived from the meteorological buoy. The rates of change of wind speed, dW_{10}/dt (m s^{-1} h^{-1}) and direction, $d\theta_{wi}/dt$ (° h^{-1}), during the recording periods are shown. The swell data are derived from the first and last 8-min sonograph and pressure records of the recording periods, the duration of which is D (h). The mean period of the swell, T_s (s), is the mean zero crossing period found from the pressure records. The mean swell height, H (m), is found from the pressure records, as in section 4d(3), and the direction, θ_s (°), is found from the sonographs [see section 4d(1)]. The swell direction could not be obtained with any confidence in winds less than 10 m s^{-1}. The periods, T_{hf} (s), and directions, θ_{hf} (°), of high-frequency waves are obtained from sonograph records. No reliable direction values could be found at the highest wind speeds when swell was dominant.

	Wind			Langmuir bands				High frequency		Swell		
D (h)	W_{10} (m s^{-1})	θ_{wi}	dW_{10}/dt (m s^{-1} h^{-1})	$d\theta_{wi}/dt$	V (cm s^{-1})	θ_b	S (m)	T_{hf} (s)	θ_{hf}	T_s(s)	θ_s	H(m)
2	3.8 ± 0.7	342 ± 14	−0.1	−3.5	15.5 ± 1.9	353 ± 23	3.6 ± 0.7	1.9 ± 0.1	326 ± 22	11.6 ± 1.4	—	0.36 ± 0.02
4	4.5 ± 0.5	358 ± 16	−0.2	−4.2	−3.8 ± 11.7	359 ± 34	3.8 ± 0.4	2.4 ±0.4	237 ± 25	11.3 ± 0.6	—	0.44 ± 0.03
4	5.8 ± 0.8	341 ± 32	−0.3	−6.7	3.4 ± 3.0	326 ± 38	4.2 ± 0.4	2.5 ± 0.6	287 ± 10	11.3 ± 0.2	—	0.66 ± 0.01
4	8.8 ± 0.9	24 ± 26	0.3	10.0	9.0 ± 9.6	32 ± 28	4.6 ± 0.5	2.9 ± 0.3	282 ± 32	11.3 ± 0.2	—	0.96 ± 0.01
4	11.6 ± 0.4	350 ± 23	0.3	7.5	7.1 ± 5.7	347 ± 33	5.4 ± 0.8	3.1 ± 0.3	271 ± 22	11.3 ± 0.5	198 ± 7	1.54 ± 0.47
2	12.7 ± 0.4	36 ± 25	0.2	4.2	0.1 ± 10.5	17 ± 16	6.0 ± 0.8	3.8 ± 0.1	—	12.8 ± 0.7	300 ± 9	1.86 ± 0.30

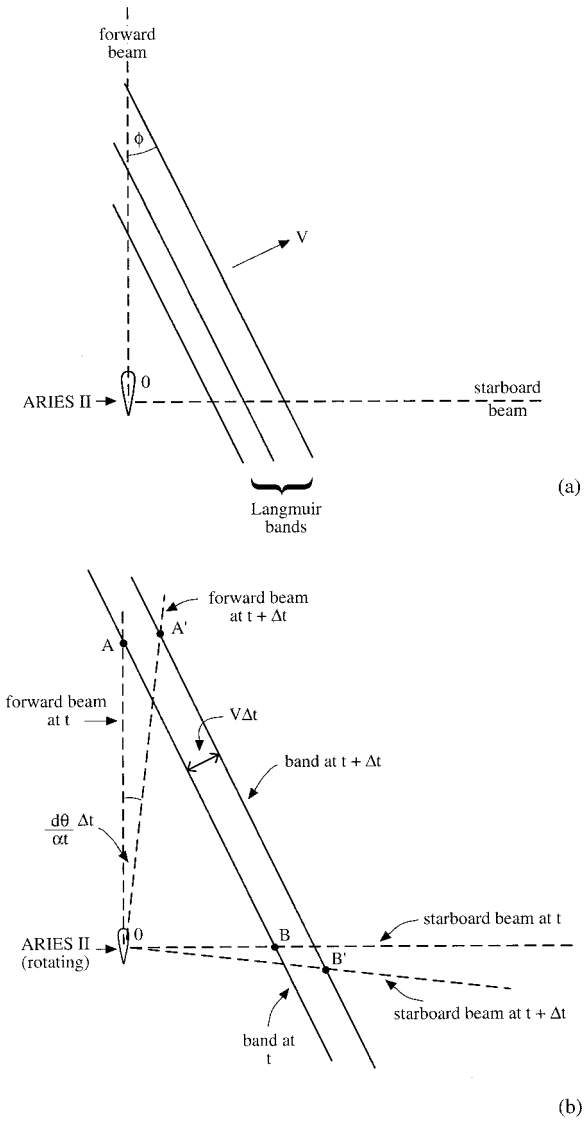

FIG. 9. Plan view geometry of a scattering band of bubbles resulting from Langmuir circulation that moves laterally—e.g., in a tidal current at speed V. In (a) the sonar beams are supposed fixed, and in (b), where a band is shown at times t (AB) and $t + \Delta t$ (A′B′), they rotate clockwise at speed $d\theta/dt$. The band has moved a distance $V\Delta t$. The apparent speed of the band along the forward beam is (OA′ − OA)/Δt, where A and A′ are the points of intersection of the forward beam with the band at times t and $t + \Delta t$. The speed along the starboard beam is (OB′ − OB)/Δt.

simultaneously in the two beams of the sonar; only the bands appearing in each have the same orientation and sideways drift speed. If, however, the sonar is rotating so that its heading is increasing at a rate $d\theta/dt$, the range of the bands in the two beams will, in general, be affected (Fig. 9b). If the speeds measured in the forward and starboard beams are then v_f and v_s, respectively, at range r (the same in each beam) the orientation angle is given by

$$\tan\phi = (v_s - Rd\theta/dt)/(v_f + Rd\theta/dt), \qquad (1)$$

where $R = (r^2 - d^2)/r$. The lateral advection speed V is given by

$$V = \frac{r[v_f v_s + R^2(d\theta/dt)^2]}{\{rR[(v_f + Rd\theta/dt)^2 + (v_s - Rd\theta/dt)^2]\}^{1/2}}. \quad (2)$$

The average distance between neighboring bands, d_f and d_s, measured in the directions of the forward and starboard sonar beams, respectively, combine to give the mean band spacing, $d_b = d_f d_s/(d_f^2 + d_s^2)^{1/2}$. The ratio d_s/d_f is equal to $\tan\phi$, and this provides a consistency check on (1).

In Fig. 7, $v_f \approx -0.09$ m s^{-1}, $v_s \approx -0.21$ m s^{-1} at $r = 120$ m, and $d\theta/dt \approx 0$ rad s^{-1}. From (1), $\phi \approx 67°$, so that, since the forward beam is pointing in direction 274° (Fig. 7d), the Langmuir bands are in direction 207°—that is, approximately in the downwind, 227° ± 20°, direction. From (2), the lateral drift speed of the bands is $V = -0.08$ m s^{-1}.

c. The effect of oscillations in beam direction on the range of linear targets

1) HEADING

Changes in the heading lead to variations in the direction in which the two sonar beams point. Suppose, for example, that a sonar beam, in its mean orientation, intersects a stationary line of scatterers, perhaps a band of bubbles resulting from bubble cloud convergence in Langmuir circulation, at range r_0 and at an angle, ϕ (as shown in Fig. 10; $r_0^2 = d^2 + OA^2$). If the beam heading oscillates so that at time t it points at an angle, $\theta = \theta_0 \sin\sigma t$, to its mean direction (i.e., in direction OA′ in Fig. 10), then it is easily shown that the range r is then given by

$$r^2 - d^2 = \frac{(r_0^2 - d^2)\sin^2\phi}{\sin^2(\phi - \theta_0 \sin\sigma t)}, \quad (3)$$

where d is the depth of the instrument. Variations are in phase at all ranges. The variation in range increases as range r_0 increases and also as ϕ decreases, or as the bands become more closely aligned to the beam direction. The effect is particularly notable in the starboard beam sonograph (Fig. 7b) (e.g., at 0–20 s when heading fluctuations are most severe).

2) PITCH

The effect of changes in pitch angle, Φ, is to cause the center of the forward sonar beam to move but not to change the intersection of the beam with the surface or the target range. However, the vertical inclination of the starboard beam will change, and its intersection with the surface will migrate sideways by a distance, $d\tan\Phi$. Fluctuations of ±2° occur in swell (Fig. 7e), leading to beam migration of typically 1.4 m at the surface.

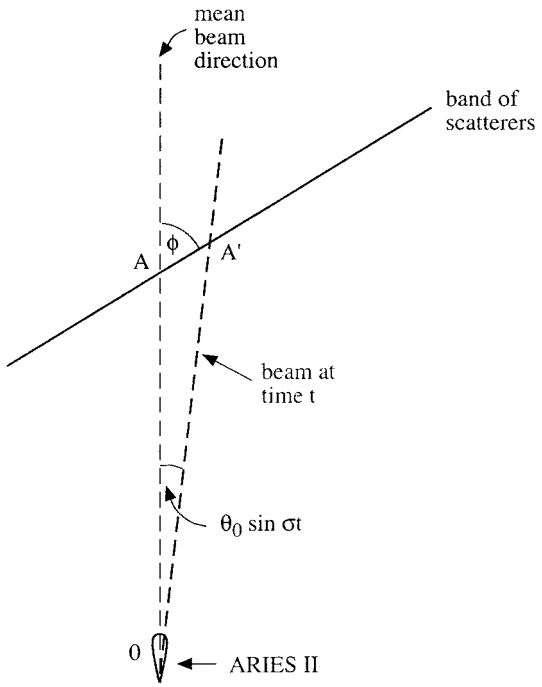

FIG. 10. Plan view geometry of a beam that intersects a line, AA′, of scatterers. The mean direction of the beam is OA, where O is the position of ARIES II. At time t the beam, OA′, makes an angle, $\theta_0 \sin\sigma t$, to the mean direction.

3) LATERAL TILT

The effects of variations are as for pitch, but with effects on the forward and starboard beams reversed. Variations are typically 1°, with corresponding lateral motions of the forward beam of 1 m, but these may be greater when internal waves are passing (see Fig. 13e).

d. The effect of surface waves

1) THE SPEED AND DIRECTION OF PROPAGATION OF THE SURFACE WAVES

If we assume that at ranges $\gg d$ the position of the scattering point on the wave surface is at fixed phase with respect to the wave crest, then the asymptotic speeds of the wave targets toward the sonar in the forward, c_f, and starboard, c_s, beams, respectively, give the phase speed, $c = c_f c_s/(c_f^2 + c_s^2)^{1/2}$, of the approaching waves (Fig. 11). The effect of beam rotation, included in section 4b, is generally negligible since $c \gg rd\theta/dt$. The direction of the wave propagation relative to that of the forward beam is $\beta = \tan^{-1}(c_f/c_s)$. The wave amplitude and period may be measured from the sonograph images of the water surface above the instrument. The wavelength may also be determined, provided that two waves are visible simultaneously in the sonographs (i.e., if the distance between crests in each beam direction is less than the range).

In Fig. 7 the swell waves of a period of approximately

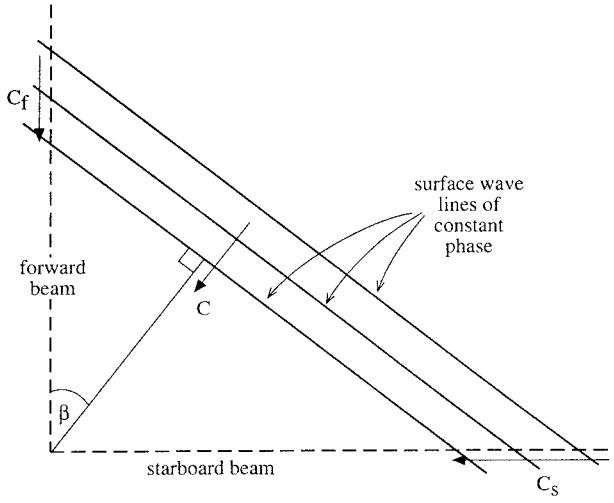

FIG. 11. Geometry of waves propagating up the sonar beams toward a point on the sea surface directly above ARIES II. The intersection of the sonar beams with the sea surface are shown, and c_f and c_s are the speeds of the lines of constant phase measured in the two beams far from the sonar.

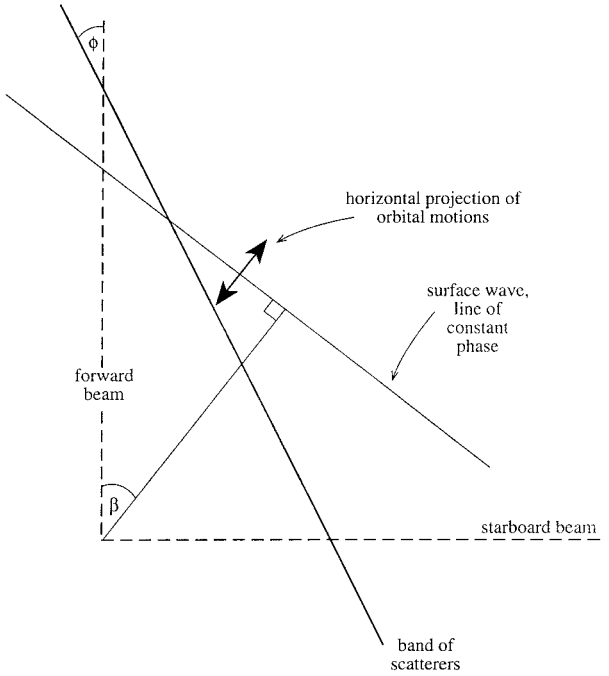

FIG. 12. Geometry of the movement of bubble clouds by waves in the two sonar beams. The band of scatterers is moved and bent by passing surface waves, changing its range in the two beams.

11 s appear to propagate down the forward beam; no evidence of propagation is evident in the starboard beam. The hyperbola overlaid on the forward sonograph (Fig. 7a) represents a target moving down the beam at the speed $c = (g/\sigma)^{1/2}$ of a surface gravity wave in deep water with frequency σ. (The corresponding wavelength is 200 m, and the deep-water wave assumption is valid.) This fits the shape of the bands quite well.

2) CURRENT FLUCTUATIONS PRODUCED BY SURFACE WAVES

According to linear theory, the horizontal current induced at a depth, d, by a surface gravity wave, $\eta = a\cos(kx - \sigma t)$, with amplitude a, wavenumber k, and frequency σ is $u = a\sigma\{\cosh[k(h - d)]/\sinh(kh)\}\cos(kx - \sigma t)$ (Kinsman 1984), where the total water depth is h. The horizontal motion is in phase with the surface elevation. If kh is large (or when the wavelength is less than about twice the water depth), $\tanh(kh)$ is approximately equal to unity and the amplitude of u is $a\sigma\exp(-kd)$. The motion is attenuated from that at the surface by a factor $\exp(-kd)$. If the depth of ARIES II is 37 m, this attenuation factor is equal to 8.8×10^{-8}, 0.017, and 0.36 for waves of 3, 6, and 12 s (corresponding wavelengths 14.0, 56.2, and 225 m), respectively.

3) PRESSURE VARIATIONS CAUSED BY WAVES

If we suppose that the vertical displacements of ARIES II caused by individual waves can be neglected in comparison with the wave amplitude, then, to the first approximation (i.e., for waves of small slope), the pressure fluctuations at the instrument resulting from waves of frequency σ and wavenumber k are in phase with the surface elevation and of amplitude $\Delta p = g\rho a\cosh[k(h - d)]/\cosh(kh)$, where h is the water depth, a is the wave amplitude, d is the instrument depth, and $\sigma^2 = gk\tanh(kh)$ is the dispersion relation (e.g., see Kinsman 1984). If kh is large, then Δp is approximately equal to $g\rho a\exp(-kd)$. The size of the attenuation factor, $\exp(-kd)$, has been considered in the section above.

In Fig. 7c, the amplitude of the largest pressure fluctuations (expressed in meters of water) is about 1 m. The attenuation factor is 0.319 for 11.3-s swell waves, so that the surface swell amplitude is 3.1 m, which is consistent with the sonographs.

4) THE MOVEMENT OF BUBBLE CLOUDS BY WAVES

The near-surface orbital motions induced by surface waves are, to a first approximation, ellipses with horizontal and vertical axes of length $[2a\coth(kh)]$ and $2a$, respectively. These will induce changes in the range of targets, such as the bubble bands, detected by the sonar. At a large range when the sonar beams intersect the surface at a small glancing angle, the main contribution to range changes comes from the induced horizontal movements. If the waves are traveling in a direction β to the forward sonar (Fig. 12), the amplitude of the change in range in the forward sonar beam of bubble bands making an angle ϕ with the forward beam is $2a\coth(kh)\sin(\beta + \phi)/\sin\phi$, provided that the band is

moved only by the orbital motions induced by the wave. The corresponding amplitude in the starboard beam is $2a \coth(kh) \sin(\beta + \phi)/\cos\phi$. Unlike the range fluctuations produced by oscillations in the heading of the sonar [section 4c(1)], these do not increase with range and will show phase advance in range at the phase speed of the waves. Examples are shown in Fig. 8 (e.g., in Fig. 8d at 1–2 min, 120–150-m range).

5. Example of some phenomena observed using ARIES II

a. Waves and wave groups

The presence of waves and wave groups is evident in the images of the sea surface in Figs. 7 and 8. Figure 7 shows that the long (order 10-s period) waves produce pressure fluctuations at the instrument [see section 4d(3)]. The currents produced by the long waves affect the orientation and tilt of the instrument [section 4d(2)], and they, rather than any inherent instability of the instrument package, generally determine the angular fluctuation variance. At low wind speeds the shorter waves of period 2–4 s can be observed in the surface echoes, and their images at a larger range can be used to determine their propagation direction [see section 4d(1)]. At higher wind speeds (>12 m s^{-1}) it becomes difficult to discriminate the shorter waves, but the directions of the long waves can then be determined from the sonographs (e.g., Fig. 7), as described in section 4d(1). Table 1 shows some analysis of waves and wind speeds from the dataset.

b. Internal waves

Figure 13 shows a typical 2-h-long record with internal waves. A relatively small temperature perturbation passes at 18 min, producing a 120° rotation in the instrument heading and a consequent alteration (the view direction is changed) in the banded Langmuir circulation patterns in the sonographs. A deep wave trough arrives at the mooring position 45 min into the record. This has a single temperature peak, in contrast with those shown in Fig. 5. The increasing temperatures marking the forward flank of the wave trough are accompanied by the approach of a scattering band in the forward sonograph. This arrives above the sonar at about 40 min, before the arrival of the wave trough, and is subsequently visible as a receding target in the starboard sonograph. The speed of this band is 0.48 ± 0.02 m s^{-1} toward $135 \pm 5°$. This is consistent with the speeds and directions of internal waves in the area (Small et al. 1998). The presence of the scattering band on the forward face of the wave is consistent with the observations of surface wave steepening and sometimes breaking in the convergence zone ahead of the internal wave trough (e.g., see Hughes and Grant 1978; Holligan et al. 1985; Thorpe et al. 1987). In an expanded-time sonograph it can be seen that there is indeed flow convergence into the band, the flow ahead being 0.33 ± 0.03 m s^{-1} and the flow behind being 0.55 ± 0.03 m s^{-1}. Assuming that the wave trough travels at the same speed as the scattering band, its width, corresponding to its time duration of 10 min (Fig. 13c), is 276 m. A farther band, although of lower-than-average scattering, suggesting shadowing, is seen receding in the starboard beam at 0.37 ± 0.03 m s^{-1} at 83–90 min, again preceding an internal wave trough. This sonar beam is in the direction $115° \pm 10°$. The forward beam may then be almost parallel to the internal wave crest. No evidence of the internal wave approach is detected in this beam. A target is also visible at 105 min when the temperature again peaks. This moves at 0.37 ± 0.03 m s^{-1} toward $110° \pm 5°$. The decreasing speeds are consistent with the evolving internal wave soliton packets in the area.

The mean heading of the instrument (Fig. 13d) is to the east, indicating a westward flow. Rapid changes in orientation (Fig. 13d) and instrument tilt (Fig. 13e) occur as the internal waves arrive. The first wave causes the instrument to orientate toward the direction from which the internal wave is inferred to have come, indicating a current pulse in the wave propagation direction, which is consistent with the currents observed in internal waves (e.g., New and Pingree 1990). The positive forward inclinometer (nose up) and negative starboard (i.e., starboard down) inclination seen as the wave passes implies that the instrument is tilted backward and to its right by the currents, the starboard inclination suggesting a failure to align perfectly or fast enough to the changing flow.

c. Langmuir circulation

Table 1 provides a summary analysis of waves and Langmuir bands in different wind conditions. The band speed, spacing, and orientation have been determined as explained in section 4b, taking measurements every 10 min from the sonographs when the bands were distinct and making no attempt to distinguish between the ''strong'' and ''weak'' bands (e.g., those visible in Fig. 7). The lateral advection V of the bands is probably dominated by tidal currents, and the sign ascribed to the right or left of the band orientation, θ_b, may have little relation to the wind. The band direction is ambiguous to a factor of 180°, and it has been chosen to be that direction closest to the wind direction with which it generally corresponds to within 20°. In determining V and θ_b, it was necessary to take into account the variation of beam heading, $d\theta/dt$ [see (1) and (2)], which contributes significantly in about 50% of the cases studied. The range of uncertainty in θ_b shown in Table 1 includes the uncertainty in estimates of $d\theta/dt$. The principal conclusion to be drawn is that within the limited dataset the band spacing increases with wind speed. Note that waves and wind are generally poorly aligned and that the Langmuir bands are better aligned to the

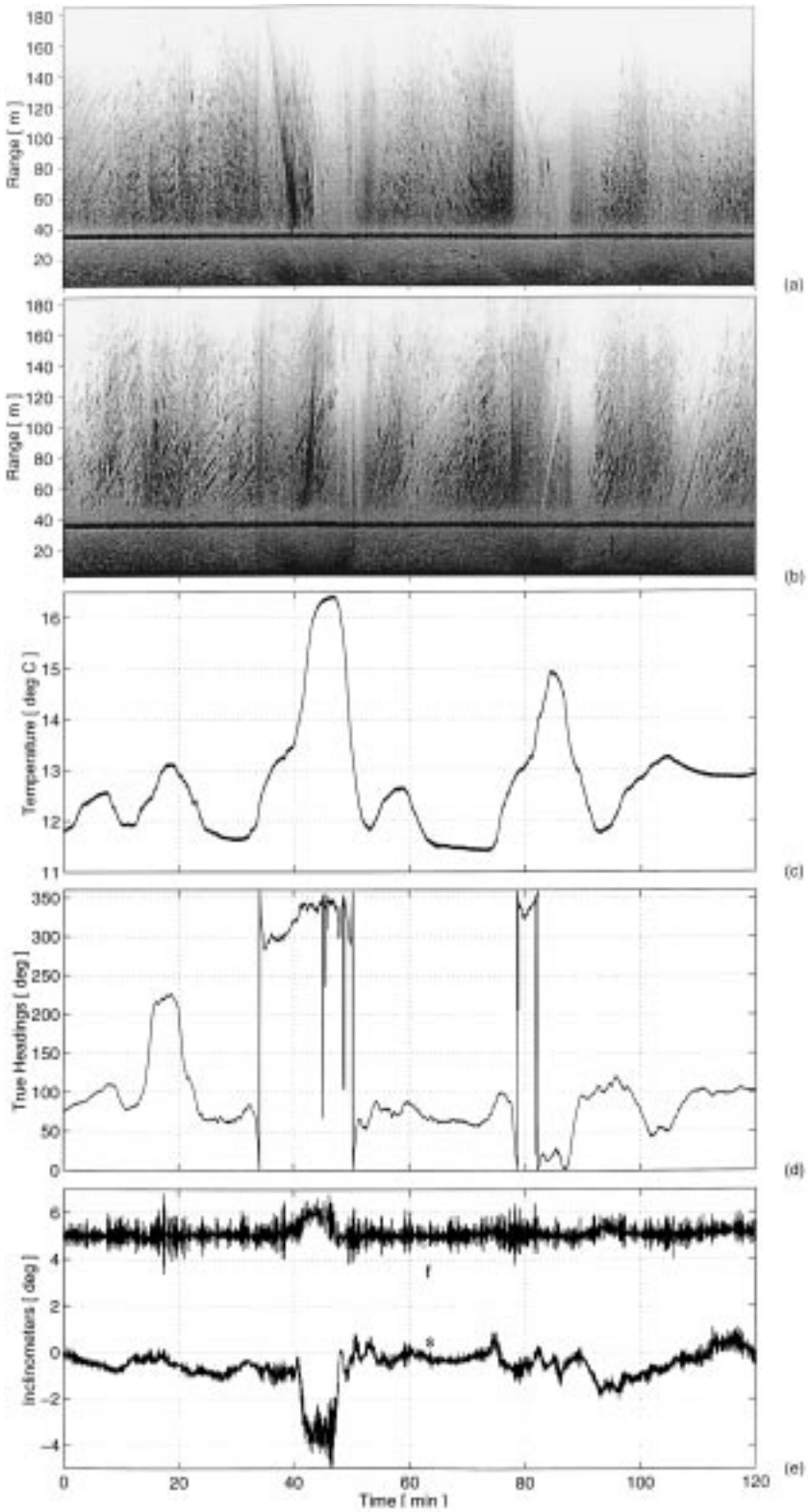

FIG. 13. Internal waves in a 2-h sonograph. (a) The forward and (b) the starboard sonographs. (c) Temperature fluctuations at ARIES II. The deepest internal wave trough occurs 45 min into the record. (d) The direction of the foreward beam and (e) the fore–aft (labeled f) and lateral (labeled s) inclinometers. The wind speed is 3.2 ± 0.3 m s^{-1} from 002° ± 16°. The record begins at 1647 GMT 21 August 1995.

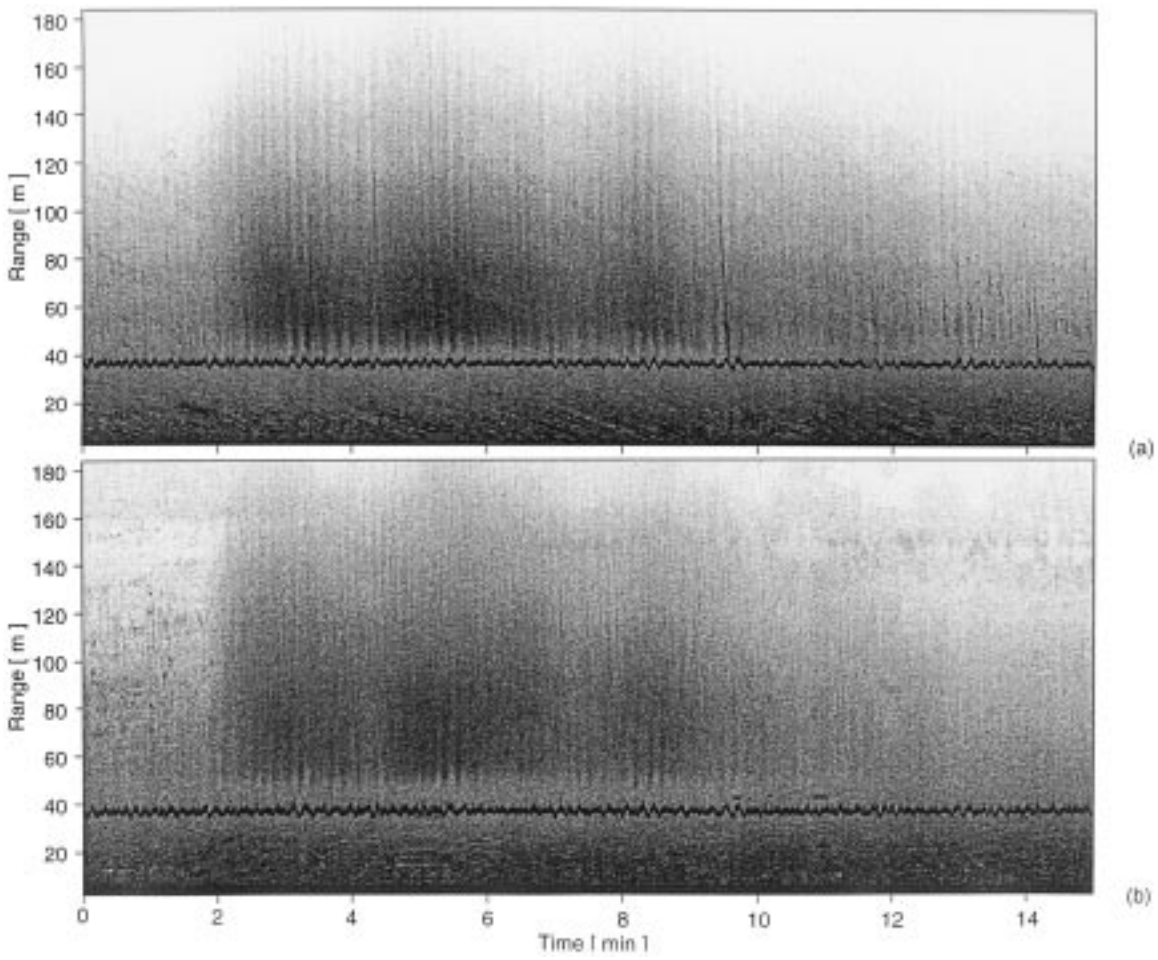

FIG. 14. Brief rain showers seen as dark vertical bands across the sonograph images beginning at 2 and 13.5 min, for example. The wind speed is 2.1 ± 0.2 m s^{-1}, veering in direction from 320° to 150°. The record begins at 0650 GMT 26 August 1995.

wind than to the wave propagation direction. Following Polonichko (1997), this may imply that the mean shear is greater than the Stokes drift shear.

d. Rain squalls

Figure 14 is an example of the effect of passing rain showers on the sonar images. Similar diffuse and nondirectional images of rain have been detected by side-scan sonar in shallow water (Thorpe and Hall 1983). The enhanced diffuse surface scattering may derive from the small-scale surface roughness elements produced by the raindrop impacts and capillary ripples or from rain-generated bubbles.

6. Conclusions

An instrument has been constructed to collect high-resolution, acoustic, side-scan images. It has been tested near the shelf break west of Scotland. Its trials demonstate that it provides novel insight into the structure and processes active in the upper ocean, particularly waves and coherent structures that result in local convergence. Analysis is currently directed toward establishing the effects of wind, swell, and internal waves on the Langmuir circulation bands (see Thorpe 1997).

Acknowledgments. Funding for the construction of ARIES II was provided by the Natural Environment Research Council (NERC) as part of its Scientific Instrument Development program for the Autosubs and LOIS (SIDAL) program under Contract GST/02/830. Funds for the trial deployment west of Scotland were also provided by NERC as part of the Land Ocean Interaction Study Shelf Edge Study (LOIS SES). Environmental and current data were supplied by the British Oceanographic Data Centre and by other participants in LOIS SES. We are most grateful for their help and cooperation. The wind speeds for the period 11–16 August 1995 were kindly provided by Dr. J. Scott, DRA, Winfrith, United Kingdom. MJU acknowledges funding from CONACYT, Mexico.

REFERENCES

Apel, J. R., J. R. Holbrook, A. K. Liu, and J. J. Tsai, 1985: The Sulu Sea internal soliton experiment. *J. Phys. Oceanogr.,* **15,** 1625–1651.

Farmer, D., and M. Li, 1994: Patterns of bubble clouds organized by Langmuir circulation. *J. Phys. Oceanogr.,* **25,** 1426–1440.

Fedorov, K. N., and A. I. Ginsberg, 1986: Phenomena on the sea surface observed visually. *Oceanology,* **26,** 5–14.

Holligan, P. M., R. D. Pingree, and G. T. Mardell, 1985: Oceanic solitons, nutrient pulses and phytoplankton growth. *Nature,* **314,** 348–350.

Hughes, B. A., and H. L. Grant, 1978: The effect of internal waves on surface wind waves. I: Experimental measurements. *J. Geophys. Res.,* **83,** 443–454.

Huthnance, J. M., 1986: The Rockall slope current and shelf-edge processes. *Proc. Roy. Soc. Edinburgh,* **88B,** 83–101.

Kinsman, B., 1984: *Wind Waves.* Dover, 676 pp.

New, A. L., and R. D. Pingree, 1990: Large-amplitude internal soliton wave packets in the Bay of Biscay. *Deep-Sea Res.,* **37,** 513–524.

Peters, A. S., and J. J. Stoker, 1960: Solitary waves in liquids having non-constant density. *Commun. Pure Appl. Math.,* **13,** 115–164.

Polonichko, V., 1997: Generation of Langmuir circulation for non-aligned wind stress and Stokes drift. *J. Geophys. Res.,* **102,** 15 773–15 780.

Sandstrom, H., and J. A. Elliott, 1984: Internal tide and solitons on the Scotian shelf: A nutrient pump at work. *J. Geophys. Res.,* **89,** 6415–6426.

Small, J., and J. Scott, 1998: Observations of large amplitude internal waves at the Malin Shelf edge during SESAME 1995. *Ann. Geophys.,* in press.

Thorpe, S. A., 1984a: On the determination of K_v in the near-surface ocean from acoustic measurements of bubbles. *J. Phys. Oceanogr.,* **14,** 855–863.

——, 1984b: The effect of Langmuir circulation on the distribution of submerged bubbles caused by breaking waves. *J. Fluid Mech.,* **142,** 151–170.

——, 1986: Measurements with an Automatically Recording Inverted Echo Sounder; ARIES and the bubble clouds. *J. Phys. Oceanogr.,* **16,** 1462–1478.

——, 1997: Interactions between internal waves and boundary layer vortices. *J. Phys. Oceanogr.* **27,** 62–71.

——, and A. J. Hall, 1983: The characteristics of breaking waves, bubble clouds, and near-surface currents observed using side-scan sonar. *Cont. Shelf Res.,* **1,** 353–384.

——, M. B. Belloul, and A. J. Hall, 1987: Internal waves and whitecaps. *Nature,* **330,** 740–742.

Zedel, L., and D. M. Farmer, 1991: Organized structures in subsurface bubble clouds: Langmuir circulation in the open ocean. *J. Geophys. Res.,* **96,** 8889–8900.